20th Australasian Fluid Mechanics Conference
Perth, Australia
5-8 December 2016

Evolution of a Modelled Hairpin Vortex in a Laminar-Boundary-Layer Flow

K. Matsuura[1]

[1]Graduate School of Science and Engineering
Ehime University, 3 Bunkyo-cho, Matsuyama, Ehime, 790-8577, Japan

Abstract

Effects of circulation on the evolution of a hairpin-like vortex tubes and the associated response of near-wall flows in the shear of laminar boundary-layer flows are investigated using a model proposed by Hon and Walker (Hon, T.L. & Walker, J.D.A, Computers & Fluids, 20(3), pp. 343–358, 1991). Direct numerical simulations with freestream Mach number of 0.5 are conducted. Numerous secondary hairpin vortices, much more than previously reported, which are regularly aligned in the streamwise direction are allowed to be newly generated according to the shear-layer instability of the legs of an initial hairpin vortex. After the generation of the secondary hairpin vortices over the hairpin legs, small-scale near-wall turbulence is produced when the circulation is sufficiently large. The largest fluctuations in streamwise velocity appear before the small-scale disturbances appear both between and around the hairpin legs. Thus, boundary-layer transition is induced rapidly starting from the hairpin-like vortex tube.

Introduction

The hairpin vortex is considered to be the basic building block commonly observed in the dynamics of transitional and turbulent flows near a wall [1]. Since the work of Theodorsen [2], there have been many studies on hairpin/horseshoe vortices. Several publications provide overviews of the formation of the hairpin vortex [3-6]. A typical symmetric hairpin vortex consists of two legs, neck and head; connected legs directed away from the wall by the head constitute a warped structure of the vortex tube. Based on the literature, a hairpin vortex has many intriguing aspects in understanding the generation of turbulence.

Moin *et al* [7] computationally studied the deformation of a hairpin-shaped vortex filament under self-induction and in the presence of shear using the Biot-Savart law, and showed a mechanism for generating ring vortices in turbulent shear flows. Acarlar and Smith [8] experimentally visualized the dynamics of hairpin vortices in the downstream wake of a hemisphere. Hon and Walker [9] developed a stable numerical method based on Lagrangian vortex method that can accurately compute the trajectory of a three-dimensional vortex having a small core radius. By the method, they showed that a two-dimensional vortex containing small three-dimensional disturbances becomes complex with subsidiary hairpin vortices forming outboard of the original hairpin vortex. Singer *et al* [10] studied the formation and growth of a hairpin vortex in a flat-plate boundary layer and its later development into a young turbulent spot. Initial hairpin vortex was triggered by fluid injection through a slit in the wall. They reported the formation of multiple hairpin vortex heads between stretched legs, new vortices beneath the streamwise-elongated vortex legs, and a traveling region of highly disturbed flow with an arrowhead shape similar to that of a turbulent spot. Zhou *et al* [11,12] studied, by direct numerical simulation (DNS), the evolution of a symmetric pair of quasistreamwise vortical structures extracted from the two-point correlation tensor of turbulent channel flow data by a linear stochastic estimation procedure. They reported that sufficiently strong hairpin vortices generate a hierarchy of secondary hairpin vortices, and the mechanism of their creation closely resembles the formation of the primary hairpin vortex. They addressed in detail the mechanisms for the autogeneration of hairpin vortices, and formulated criteria for the generation of new hairpins, in terms of the strength and location of the initial hairpin. Liu *et al* [13] conducted a compressible DNS for non-linear stages of laminar-turbulent transition. They discussed the coherent vortex structure appearing in the late stages of transition and the mechanism of formation of single vortex ring, multiple vortex rings, and small length scale. At the inflow, they assumed two-dimensional waves and a pair of oblique waves in addition to the laminar boundary layer profile to reproduce transition of *K*-regime. Duguet *et al* [14] investigated the region of phase space separating transitional from relaminarizing trajectories regarding the Blasius boundary layer, and a quasicyclic mechanism for the generation of hairpin vortex offspring. Cohen *et al* [15] proposed a model consisting of minimal flow elements that can produce packets of hairpins. They showed that the three components of the model are simple shear, a counter-rotating vortex pairs having finite streamwise vorticity magnitude and a two-dimensional wavy (in the streamwise direction) spanwise vortex sheet. Eitel-Amor *et al* [16] studied the characteristics of hairpin vortices in turbulent boundary layers by parallel and spatially developing simulations. They found that secondary hairpins are only created shortly after initialization, with all rotational structures decaying for later times. They also reported that the regeneration process is rather short-lived and may not sustain once a turbulent background is developed. Sabatino *et al* [17] studied experimentally hairpin vortex formation in a laminar boundary layer by fluid injection through a narrow slot. They discussed hairpin vortex head, legs and secondary hairpin vortex focusing on its circulation strength.

Although there are many studies on hairpin vortices, effects produced by varying the physical parameters associated with the hairpin vortices on its stability and near-wall dynamics have not necessarily been investigated separately and systematically. In this regard, the hairpin model proposed by Hon and Walker [9] is particularly intriguing because the degrees of freedom of the system such as vortex curve, circulation, size, angle-to-wall, core radius of a vortex cross-section, and background velocity field appears to enable a systematic investigation directly. However, the model has not been studied in detail within the framework of DNS. Recently, the present author [18] conducted a DNS on the dynamics of single hairpin vortex and a straight vortex tube using the model. However, the process of transition is not discussed in details. Therefore, in this study, the process is discussed in details using the results of the DNS. The focus is on the effects of circulation.

Computational Method

Freestream Mach number is 0.5 and streamwise Reynolds number at the inlet is 5.34×10^5. At the initial time t=0, single hairpin vortex or a straight vortex tube of finite length is embedded in a laminar boundary layer. The vortex axes of the legs of the hairpin vortex and the straight vortex tube are inclined to the x(streamwise) axis and its angle is 4°. Computation is impulsively started from the initial condition. Three kinds of circulation magnitudes are considered in this study. The circulations of the vortex $\Gamma/(2\pi)$ non-dimensionalized by freestream velocity and the displacement thickness δ_{in}^* at the inlet, denoted as Γ^*, is chosen as 6.24, 12.4 and 24.9. Velocity fields induced by the vortex tubes are generated by the algorithm of Hon and Walker [9] explained by the eqns. (1-3). The algorithm is a modification of the Moore's algorithm [19] which is reported to exhibit strong numerical instability for small value of a core radius a. At an arbitrary location in space X_0, velocity field u due to a vortex is basically described by the Biot-Savart Law. Contour C is a curve defining a vortex tube, and Γ is circulation about the vortex core, and u_{ext} is a background velocity field.

$$\boldsymbol{u}(\boldsymbol{X}_0) = -\frac{\Gamma}{4\pi}\int_C \frac{(\boldsymbol{X}_0 - \boldsymbol{X})}{\left|\boldsymbol{X}_0 - \boldsymbol{X}\right|^3}\times d\boldsymbol{X} + \boldsymbol{u_{ext}}(\boldsymbol{X}_0), \qquad (1)$$

When X_0 is close to the curve C, the above equation is switched to the following equation to prevent singularity. The parameter s is a Lagrangian coordinate which ranges from -∞ to ∞ along the vortex. The integrand of $R(s,s_0)$ is shown in [9].

$$\boldsymbol{u}(s_0) = \frac{\Gamma}{4\pi}\int_C R(s,s_0)ds + \frac{\Gamma}{4\pi}\left(\frac{\partial \boldsymbol{X}}{\partial s}\right)_0 \times \left(\frac{\partial^2 \boldsymbol{X}}{\partial s^2}\right)_0 \int_C P(s)ds + \boldsymbol{u_{ext}}, \qquad (2)$$

$$P(s) = \frac{\frac{1}{2}(s-s_0)^2}{\left[(s-s_0)^2\left(\frac{\partial \boldsymbol{X}}{\partial s}\right)_0^2 + \mu^2\right]^{3/2}}, \qquad (3)$$

$$\mu = \exp(-3/4)a, \quad a = 0.25$$

The initial vortex configuration used in the case of the single hairpin vortex is of the form

$$\boldsymbol{X}(s) = A(\boldsymbol{i}\cos\alpha + \boldsymbol{j}\sin\alpha)\exp(-\beta s^2) + \boldsymbol{j} + s\boldsymbol{k} \qquad (4)$$

Here, $\boldsymbol{i}, \boldsymbol{j}, \boldsymbol{k}$ are unit vectors in corresponding to the streamwise (x), normal (y) and spanwise (z) directions, respectively. Eq. (4) represents a two-dimensional vortex located a unit distance from the wall with a three-dimensional distortion which is symmetrical about s=0. In addition, A represents the amplitude of the distortion and α is the angle that the plane of the distortion makes with the wall. β is a (large) number determining the effective spanwise width of the initial distortion. Here, A is $24\delta_{in}^*$. (x_c, y_c, z_c) is the root position of the vortex tube. x_c is $30\delta_{in}^*$ downstream of the inlet and y_c=$0.4\delta_{in}^*$. φ is an angle of inclination to the wall and φ=4°.

The governing equations are the unsteady three-dimensional fully compressible Navier-Stokes equations in general coordinates (ξ, η, ζ). The perfect gas law closes the system of equations. Viscosity is evaluated by Sutherland's formula and a constant Prandtl number of Pr=0.72 is assumed. The equations are solved using the finite-difference method. Spatial derivatives that appear in the metrics, convective and viscous terms are evaluated using the sixth-order tridiagonal compact scheme [20]. Near boundaries, the fourth-order one-sided and classical Padé schemes are used on the boundaries and at one point internal to them. Time-dependent solutions to the governing equations are obtained using the third-order explicit Runge-Kutta scheme. The time increment is constant and set to $\Delta t = 42.4\times10^{-4}\delta_{in}^*/u_\infty$ in all flow fields. Here, δ_{in}^* is the inflow displacement thickness which will be mentioned later, and u_∞ is the free-stream velocity. For the present computation, the Courant-Friedrichs-Lewy (CFL) number, which is defined by the maximum sums of a contravariant velocity and the speed of sound scaled by the metrics as is around 0.4. In addition to the above-mentioned spatial discretization and time integration, a tenth-order implicit filtering [21] is introduced to suppress numerical instabilities that arise from central differencing in the compact scheme. The filter parameters that appear in the left-hand side are set to 0.33 for i=2 and i_{max}-1 and 0.492 for 2 < i<i_{max}-1. Near the boundaries, implicit filters of orders p=(4,4,6,8,10) for i=(2,…,6) and i=(i_{max}-1,…,i_{max}-5), are used. The present numerical method has been well validated for the prediction of transitional and turbulent subsonic flows [22,23].

Results and Discussion

Figure 1 shows time sequence of the vortex deformation and the dynamic response of the boundary layer for Γ^*=6.24-24.9. When Γ^* =6.24, i.e., the circulation is small, small number of hairpin vortices are generated. When Γ^* =12.4, i.e., the circulation is medium, aligned hairpin vortices over the hairpin legs and turbulent regions consisting of hairpin vortices are generated. Especially at t^*=174, numerous secondary hairpin vortices much more than previously reported, which are regularly aligned in the streamwise direction, are allowed to be newly generated according to the shear-layer instability of the legs of an initial hairpin vortex [18]. Here, t^* is time non-dimensionalized by δ_{in}^* and the speed of sound c_∞. When Γ^* =24.9, i.e., the circulation is large, quasi-streamwise vortices appear near the upstream root of the legs. In addition to the central region sandwiched between the two legs, hairpin vortices are generated near the root of the two legs. Near the tail of the turbulent spot, the region of hairpin vortices are divided into two regions corresponding to the hairpin legs at t^*=87-174.

Figure 2 shows time variation of the boundary layer profiles both at $112\delta_{in}^*$ downstream of the inlet and at the spanwise center of the computational domain. When Γ^* =6.24, the profiles swell inside the boundary layers as the passage of the hairpin vortices. However, after that, the profiles come back to the original laminar boundary layer profiles. When Γ^* =24.9, the original boundary layer profiles including freestream regions are greatly modified due to the passage of the turbulent region. After t^*=147, streamwise velocity near the wall becomes large showing that the near-wall flows become turbulent.

Figure 3 shows time variation of the spanwise distribution of the streamwise velocity both at $112\delta_{in}^*$ downstream of the inlet and at the height of 10% of the local boundary layer thickness δ_{99}. When Γ^* =6.24, a low-speed region between the hairpin legs and two high-speed regions outside the low-speed regions are formed. When Γ^* =12.4, the growth of short disturbances not only in the interior region between the hairpin legs but also in the leg regions is confirmed. Before short disturbances appear both between and around the hairpin legs, i.e., around t^*=287, the streamwise fluctuations become largest around z=$8.31\delta_{in}^*$ and $13.6\delta_{in}^*$.

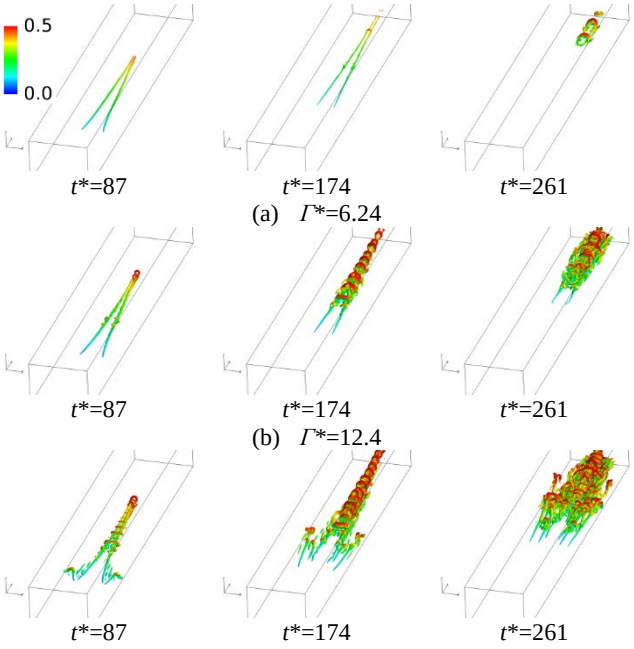

Figure 1 Time sequence of the deformation of the single hairpin vortex and the dynamic response of the boundary layer. The color shows a streamwise velocity divided by a sound speed, i.e, Mach number. [18]

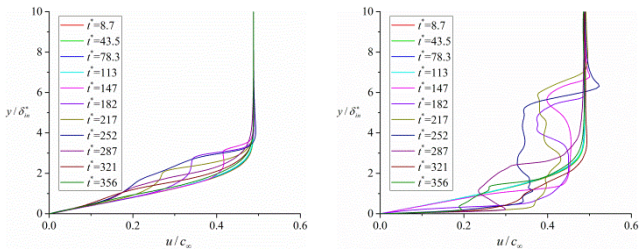

Figure 2 Time variation of the boundary layer profiles both at $112\delta_{in}^{*}$ downstream of the inlet and at the spanwise center of the computational domain

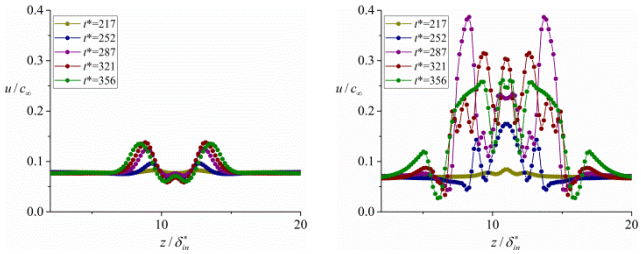

Figure 3 Time variation of the spanwise distribution of the streamwise velocity both at $112\delta_{in}^{*}$ downstream of the inlet and $y=0.1\delta_{99}$.

Conclusions

Effects of the circulation on the evolution of vortex tubes and associated response of near-wall flows in the shear of laminar boundary-layer flows were investigated by DNS using the hairpin vortex model proposed by Hon and Walker. Dynamics of single hairpin vortex was investigated. Numerous secondary hairpin vortices much more than previously reported, which are regularly aligned in the streamwise direction and bridging over the legs, are allowed to be newly generated according to the shear-layer instability of the legs of an initial hairpin vortex. After the generation of the secondary hairpin vortices over the hairpin legs, small-scale near-wall turbulence is produced when the circulation is sufficiently large. The largest fluctuations in streamwise velocity appear before the small-scale disturbances appear both between and around the hairpin legs. Thus, boundary-layer transition is induced rapidly starting from the hairpin-like vortex tube.

Acknowledgments

This work was supported by Grant for Basic Science Research Projects from the Sumitomo Foundation and the Institute of Statistical Mathematics (ISM) Cooperative Research Program 2016 ISM-CRP2019. Computational resources are provided by ISM and Japan Aerospace Exploration Agency (JAXA).

References

[1] Smith, C.R., et al., On the Dynamics of Near-Wall Turbulence, *Philos. Trans. R. Soc. London, Ser. A*, **336**, 1991, 131-175.
[2] Theodorsen, T., Mechanism of Turbulence, *Proc. of Second Midwestern Conf. on Fluid Mech., Bull.*, **149**, Ohio State Univ., Columbus, Ohio, 1952.
[3] Panton, R., Overview of the Self-Sustaining Mechanisms of Wall Turbulence, *Prog. Aero. Sci.*, **37**, 2001, 341-381.
[4] Adrian, R.J., Hairpin Vortex Organization in Wall Turbulence, *Phys. Fluids*, **19**, 2007, 041301.
[5] Lee, C.B. & Wu, J.Z., Transition in Wall-Bounded Flows, *Appl. Mech. Rev.*, **61**, 2008, 030802-1-21.
[6] Dennis, D.J.C., Coherent Structures in Wall-Bounded Turbulence, *Ann. Brazil. Acad. Sci.*, **87**(2), 2015, 1161-1193.
[7] Moin, P., Leonard, A. & Kim, J., Evolution of a Curved Vortex Filament into a Vortex Ring, *Phys. Fluids*, **29**(4), 1986, 955-963.
[8] Acarlar, A. & Smith, C., A Study of Hairpin Vortices in a Laminar Boundary Layer. Part I. Hairpin Vortices Generated by a Hemisphere Protuberance, *J. Fluid Mech*., **175**, 1987, 1-41.
[9] Hon, T.L. & Walker, J.D. A, Evolution of Hairpin Vortices in a Shear Flow, *Comput. Fluids*, **20**(3), 1991, 343-358.
[10] Singer, B.A. & Joslin, R.D., Metamorphosis of a Hairpin Vortex into a Young Turbulent Spot, *Phys. Fluids*, **6**(11), 1994, 3724-3736.
[11] Zhou, J., Adrian, R.J., Balachander, S., Autogeneration of Near-Wall Vortical Structures in Channel Flow, *Phys. Fluids*, **8**(1), 1996, 288-290.
[12] Zhou, J., Adrian, R.J. & Balachandar, S., Mechanisms for Generating Coherent Packets of Hairpin Vortices in Channel Flow, *J. Fluid Mech.*, **387**, 1999, 353-396.
[13] Liu, C. & Chen, L., Parallel DNS for Vortex Structure of Late Stages of Flow Transition, *Comput. Fluids*, **45**, 2011, 129-137.
[14] Duguet, Y., Schlatter, P., Henningson, D. & Eckhardt, B., Self-Sustained Localized Structures in a Boundary-Layer Flow, *Phys. Rev. Lett.*, **108**, 2012, 044501.
[15] Cohen, J., Karp, M. & Hehta, V., A Minimal Flow-Elements Model for the Generation of Packets of Hairpin Vortices in Shear Flows, *J. Fluid Mech.*, **747**, 2014, 30-43.
[16] Eitel-Amor, G., Flore, O. & Schlatter, P., Hairpin Vortices in Turbulent Boundary Layers, *J. Phys.: Conf. Ser.*, **506**, 2014, 012008.
[17] Sabatino, D.R. & Maharjan, R., Characterizing the Formation and Regeneration of Hairpin Vortices in a Laminar Boundary Layer, *Phys. Fluids*, **27**, 2015, 124104.
[18] Matsuura, K., Direct Numerical Simulation of a Straight Vortex Tube in a Laminar Boundary-Layer Flow, *Int. J. Compt. Methods & Exp. Meas.*, 2016, to appear.
[19] Moore, D.W., Finite Amplitude Waves on Aircraft Trailing

Vortices, *Aero. Quart.*, **23**, 1972, 307-314.
[20] Lele, S.K., Compact Finite Difference Schemes with Spectral-Like Resolution, *J. Comput. Phys.*, **103**(1), 1992, 16-42.
[21] Gaitonde, D.V. & Visbal, M.R., Padé-Type Higher-Order Boundary Filters for the Navier-Stokes Equations, *AIAA J.*, **38**(11), 2000, 2103-2112.
[22] Matsuura, K. & Kato, C., Large-Eddy Simulation of Compressible Transitional Flows in a Low-Pressure Turbine Cascade, AIAA J., **45**(2), 2007, 442-457.
[23] Matsuura, K. & Nakano, M., A Throttling Mechanism Sustaining a Hole Tone Feedback System at Very Low Mach Numbers, *J. Fluid Mech.*, **710**, 2012, 569-605.